Carbon 138 (2018) 337–347

Contents lists available at ScienceDirect

Carbon

journal homepage: www.elsevier.com/locate/carbon

Revealing hidden endotherm of Hummers' graphene oxide during low-temperature thermal reduction

Yang Shen [a], Vittorio Boffa [a, **], Ingrid Corazzari [b], Ang Qiao [c], Haizheng Tao [c], Yuanzheng Yue [a, c, *]

[a] Department of Chemistry and Bioscience, Aalborg University, 9220 Aalborg, Denmark
[b] Dipartimento di Chimica, Universitá di Torino and G. Scansetti Interdepartmental Centre for Studies on Asbestos and Other Toxic Particulates, 10125 Torino, Italy
[c] State Key Laboratory of Silicate Materials for Architecture, Wuhan University of Technology, 430070 Wuhan, China

ARTICLE INFO

Article history:
Received 2 January 2018
Received in revised form
4 April 2018
Accepted 8 May 2018
Available online 10 May 2018

Keywords:
Graphene oxide
Thermal reduction
Low temperature
Hidden endotherm
Dynamics and kinetics

ABSTRACT

Graphene oxide (GO) is a promising precursor material for fabricating graphene-like structures. However, the detailed kinetics and dynamics of GO thermal reduction still need to be revealed. Here, we present a new insight into low-temperature thermal reduction of Hummers' GO. During the low-temperature thermal treatment, the decomposition process of functional groups of Hummers' GO is found to consist of 4 steps (Step 1: below 160 °C, Step 2: between 160 and 210 °C, Step 3: between 210 and 300 °C, Step 4: above 300 °C). We discovered that Step 3 is an endothermic process. This finding differs from the common view that the thermal reduction of Hummers' GO is only an exothermic event. In addition, gaseous aromatic by-products form below 300 °C, implying that the basal carbon network could start to decompose at such low temperatures. This is in contrast to the former experimental finding that the GO carbon plane decomposes only at higher temperature (above 350 °C). Finally, based on the combined kinetic and compositional measurements, we observe the evolution of functional groups during heat-treatment, and thereby, reveal the mechanism of low temperature reduction of Hummers' GO.

1. Introduction

Graphene-based materials have been attracting considerable interest owing to their two-dimension structure (one atom thick planar sheet [1]) and outstanding properties such as: impermeability to all standard gases [2], unique electrical properties [3] inherent mechanical strength [4] and large surface area [5]. These remarkable properties make graphene-based materials attractive for a wide range of applications, encompassing contaminant adsorption, photocatalytic materials, membranes, sensors and capacitors [6–16].

Graphene oxide (GO) is an oxidized form of graphene, which normally contains four kinds of functional groups: hydroxyl, carboxyl, carbonyl and epoxide, on the carbon sheet surface [17]. The most attractive feature of GO is its ready conversion to graphene-like structure through chemical, thermal or electrochemical (partial) removal of functional groups. The reduced GO is considered as an appropriate intermediate for the large-scale production of graphene-based materials [18–22]. Thus, various reduction techniques [23–26], e.g., high vacuum, reducing gases (H_2), HCl solution, have been used to fabricate highly reduced GO. However, reduced GO products always contain residual oxygen or structural defects. In some cases, such defects may be used to tune properties of the final materials. For instance, Nair et al. reported that the spacing between two adjacent layers in GO membranes is larger than that in graphite since the former contains functional groups [11,12,27]. Hence, GO membranes possess outstanding water permeability and exceptional molecular separation properties. Eda et al. [28] observed blue photoluminescence from GO thin films after controlled reduction, thus providing novel and promising materials for optoelectronics.

In this context, it is important to establish simple and reproducible methods for the large-scale fabrication of reduced GO with desired structure and properties. To do so, we need to clarify two key

* Corresponding author. Department of Chemistry and Bioscience, Aalborg University, 9220 Aalborg, Denmark.
** Corresponding author. Department of Chemistry and Bioscience, Aalborg University, 9220 Aalborg, Denmark.
E-mail addresses: vb@bio.aau.dk (V. Boffa), yy@bio.aau.dk (Y. Yue).

https://doi.org/10.1016/j.carbon.2018.05.018
0008-6223/

questions: (1) What are the reduction mechanisms? (2) How can the reduction degree be controlled? A controllable functionalization can enable us to obtain graphene-like structures through an economically effective way, and to tailor the properties of GO for specific applications. Indeed, using different synthetic approaches, GO with different functional groups and density can be derived [17]. Hummers' method [29] and its modified versions, which involves $KMnO_4$ and H_2SO_4, are today widely used for GO synthesis, due to their simplicity and high conversion efficiency. Since the chemical structure and the stability of these functional groups remain elusive, a systematic study of the physical principle of the method, by-products and the mechanism of reduction process would be a key for realizing large-scale production of GO. Hummers' GO involves multiple reaction steps such as removal of intercalated H_2O molecules and oxide groups and the partial degradation of the basal carbon plane at high temperature. Indeed, there are a number of papers about GO reduction [18,23], however, most of the previous studies mainly focus on the high temperature (above 200 °C) reduction of GO. The low temperature (between 100 and 200 °C) degradation processes have not been well investigated. Moreover, such studies often deal with the thermal stability and chemical evolution of GO, but the thermal kinetics and dynamic evolution of the chemical reactions during annealing treatment has not been clarified.

In this study, we explore the reduction mechanism and kinetics of Hummers' GO at various temperatures between 120 and 200 °C for different annealing durations (0.5, 1, 3, 7 and 24 h). We investigate the endothermic process, which is shadowed by a strong exothermic transition. Such endothermic process may be decoupled from the exothermal response to decomposition of the carboxyl and epoxy groups, after partial reduction of GO at mild temperatures. Thus, the reduction process of multilayer GO, as observed from the DSC results, could be divided into four steps. Each step corresponds to the decomposition of different functional groups, indicating different chemical mechanisms. In this paper, we discuss the detailed thermokinetics of different decomposition steps. In addition, we analyze the release of some toxic derivatives, like SO_2 and some aromatic products (benzene et al.), which are developed in non-negligible quantities below 300 °C, while, according to the common view, only CO_2, CO and H_2O would be released during reduction at such low temperature. We study the chemical and structural evolution and the formation of a variety of GO derivatives during a controlled thermal reduction process. We attempt to offer a reasonable interpretation for the low temperature thermal reduction of graphene oxide.

2. Experimental

2.1. Graphene oxide synthesis

The graphene oxide was synthesized using Hummers' method [24,29]. All the chemicals used for the synthesis were purchased from Sigma-Aldrich, unless otherwise specified. 2.0 g natural graphite (Graphit Kropfmühl GmbH) and 1.0 g $NaNO_3$ (99%) were stirred with 50 ml sulfuric acid (98%) in a 1 L beaker. The mixture was placed in an ice bath and stirred until homogeneity. 7.0 g potassium permanganate (99%) was added slowly to avoid a sudden temperature increase. Then, the beaker was placed into a water bath at 35 °C for 1 h and a thick dark green paste was obtained. The reaction flask was poured into 80 mL deionized water slowly in order to prevent an uncontrolled temperature increase and heated to 95 °C for 30 min and get a dark brown suspension. After adding 500 mL of deionized water, followed by 6 mL of 30% H_2O_2 solution, the mixture's color changed into light yellow. After that, the suspension was washed with 200 mL HCl (5%) one time, and with 500 mL deionized water 5 times. The so obtained graphene oxide (GO) slurry was freeze-dried in a vacuum machine for 48 h to yield a fine GO powder. Synthesis and washing procedures were repeated six times starting from the same graphite sample. For each synthesis, the complete conversion of graphite to GO was checked by XRD analysis. The synthetized materials were mixed together to obtain a single raw GO powder. Such powder was divided into 0.2 g samples, which were thermally treated at 120, 140, 160, 180 and 200 °C under an argon flow for different durations (0.5, 1, 3, 7 and 24 h).

2.2. Characterization

Differential scanning calorimetry (DSC) and thermogravimetry (TG) measurements were performed on a Simultaneous Thermal Analyzer 449C Jupiter (Netzsch, Germany). The GO samples (ca. 4.5 mg) were placed into a platinum crucible at room temperature. In the dynamic measurements, the samples were held for 5 min at an initial temperature of 40 °C, then heated to 600 °C at a rate of 10 °C/min in an argon atmosphere. To examine the influence of the heating rate on the characteristic temperatures of chemical reactions, two samples, i.e. original GO and 160 °C-24 h GO, were also analyzed at 5 and 15 °C/min in an argon atmosphere. The area (enthalpy) of the calorimetric peaks was determined by using the software NETZSCH Proteus Thermal Analysis. The onset of TG curves was set at 40 °C (mass = 100%). Isothermal gravimetric measurements were also performed in an argon atmosphere on GO samples of ~4.5 mg, which were heated to the target temperature at a rate of 40 °C/min and held for 24 h.

A combined technique of the time-resolved infrared spectrometry – thermogravimetry - mass spectrometry (FTIR-TG-MS) was used to assess the species evolved during the thermal reaction. The GO samples (ca. 2 mg) were placed in an open platinum pan and heated from 30 to 700 °C at 20 °C/min under dynamic nitrogen atmosphere in a Pyris TG (PerkineElmer, USA). The gas evolved during the heating ramp was piped (gas flow 65 mL/min) via a pressurized transfer line (Redshift S.r.l., Italy) and analyzed continuously by FTIR (Spectrum 100, Perkin Elmer), equipped with a thermostatic conventional gas cell. Temperature/time-resolved spectra were acquired in the 4000-600 cm^{-1} wavenumber range and analyzed with the Spectrum software (Perkin Elmer). Temperature-resolved infrared profiles of each single moiety desorbed from samples were obtained from the intensity of a representative peak of the investigated species. The assessment of some organic species (namely benzene, stryrene, naphthlene and phenanthrene) released during the heating ramp was carried out by mass spectrometry employing the Clarus 560S mass spectrometer (PerkineElmer, USA) operated in selected ion recording (SIR) mode. The samples were heated at 20 °C/min from 30 to 400 °C. The chosen temperature range encompasses the boiling temperature of the selected organic species (namely 80.1, 145, 218 and 340 °C for benzene, stryrene, naphthlene and phenanthrene, respectively). The chromatograms were obtained by monitoring the most abundant peak (base peak) for each of the selected organic molecule, namely 78, 104, 128, and 178 m/z for benzene, styrene, naphthalene and phenanthrene, respectively.

The high sensitivity Pyrolysis-Gas chromatography–mass spectrometry (Pyr-GC-MS) was performed to detect the organic species. A CDS Pyroprobe 1500 (Analytical Inc., USA) filament pyrolyzer was directly connected to the 6890N Network GC-MS system (Agilent Technologies, USA). The GC system used a methylphenyl-polysiloxane cross-linked 5% phenyl methyl silicone (30 m, 0.25 mm i.d., 0.25 μm film thickness) capillary column. The GO samples was heated at 300 °C for 30 s in the pyrolyzer and used helium (1.0 ml/min) as the carrier gas, and split ratio was 1/20 of the total flow. The mass spectrometer coupled to the GC system was a 5973 Network Mass Selective Detector (Agilent Technologies,

USA). Mass spectra were acquired in the range 40–600 *m/z* and under electron impact at 70 eV. All instruments were controlled by Enhanced Chem Station (ver. 9.00.00.38) software.

Fourier transform infrared spectroscopy (FTIR) analysis was performed using Varian 660-IR spectrometer (Agilent, USA) at room temperature. The pellets for FTIR test were prepared by 1 mg GO grinded with 200 mg dried KBr (99.5%, Merck) for each sample. The KBr was dried at 100 °C for over 24 h. The scan range was 4000–400 cm^{-1}.

X-ray photoelectron spectroscopy (XPS) was performed by using ESCALAB 250Xi spectrometer (ThermoFisher Scientific, USA) with non-monochromatic Al Kα X-ray (1486.6 eV) at pass energy of 50 eV. The obtained C1s and O1s spectrum were fitted by using PeakFit software.

Elemental Analysis (EA) was performed by using SeriesIICHNS/O Analyzer-2400 (PerkinElmer, USA). Three copies of each GO sample were prepared with around 5 mg for each one. The average data were calculated based on the 3 repetitions.

3. Results and discussion

3.1. Hidden endothermic process

Fig. 1 shows the dynamic TG and DSC data (obtained at the heating rate of 10 °C/min) of three GO samples: the as synthetized sample and the two samples that are annealed at 160 °C for 1 h (160 °C-1 h) and 24 h (160 °C-24 h), respectively. The original GO sample shows the typical DSC and TG profiles, i.e., 4 distinct steps in the TG curves: Step 1 below 160 °C, Step 2 between 160 and 210 °C, Step 3 between 210 and 300 °C, Step 4 above 300. The mass loss below 160 °C (Step 1) is due to the endothermic evaporation of physisorbed and nanoconfined water [30]. The major loss of the mass (Steps 2 and 3) has often been ascribed to the exothermic degradation of the functional groups on graphene oxide between 160 and 300 °C [24,31–34]. The small mass loss above 300 °C (Step 4) is assigned to the basal carbon network degradation and to the removal of the most stable oxygen functionalities [35]. As expected, the TG and DSC curves of the 160 °C-1 h and 160 °C-24 h show a mass drop and an exothermal response, respectively, since part of the organic groups is degraded during thermal reduction. However, the DSC curves of the two annealed GO samples have a different profile. Indeed the combined analysis of the mass loss and heat flow curves shows two distinct phenomena: (1) a strongly exothermic process between 160 and 210 °C, and (2) a clear endothermic peak between 210 and 300 °C, as highlighted by the blue circle in Fig. 1. This endothermic peak is evident in the DSC curve of the sample 160 °C-24 h, for which no mass loss or exothermic transitions are observed in the Step 2 (160–210 °C). We infer that the original GO and 160 °C-1 h curves actually also have this endothermic transition, but in the DSC scan, it is hidden by the large exothermic peak

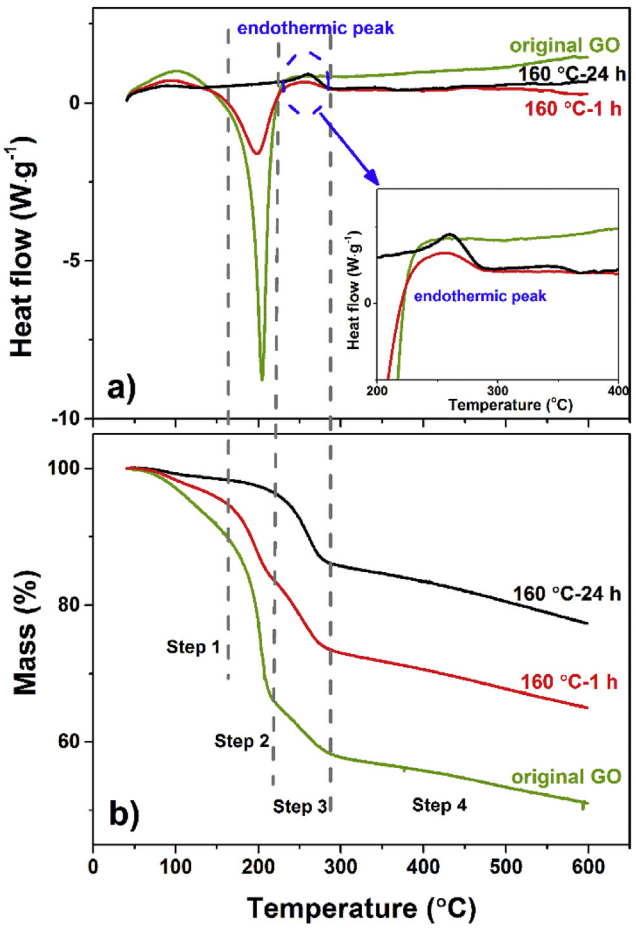

Fig. 1. DSC and TG curves of three GO samples: original, 160 °C-1 h and 160 °C-24 h. The dashed lines are used for helping distinguish the reaction steps. The blue dashed circle shows the endothermic peak. (A colour version of this figure can be viewed online.)

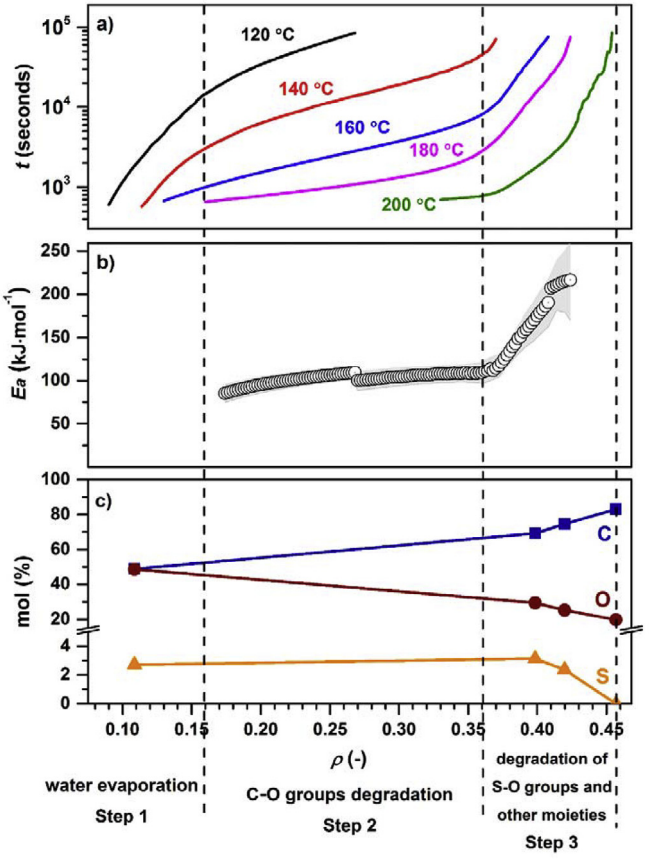

Fig. 2. Isothermal Gravimetric Analysis of GO (a) and the activation energy of the degradation process as calculated by the Mac Callum method (b). The change in slop of the isothermal gravimetric analysis and the variation of the apparent activation energy of the GO degradation are plotted as a function of the degradation degree of GO (ρ). Thus, three distinct steps, based on the literature values and the elemental analysis data (c), are here assigned to the water evaporation, decomposition of oxygen functions, and decomposition of sulfates and other moieties, respectively. (A colour version of this figure can be viewed online.)

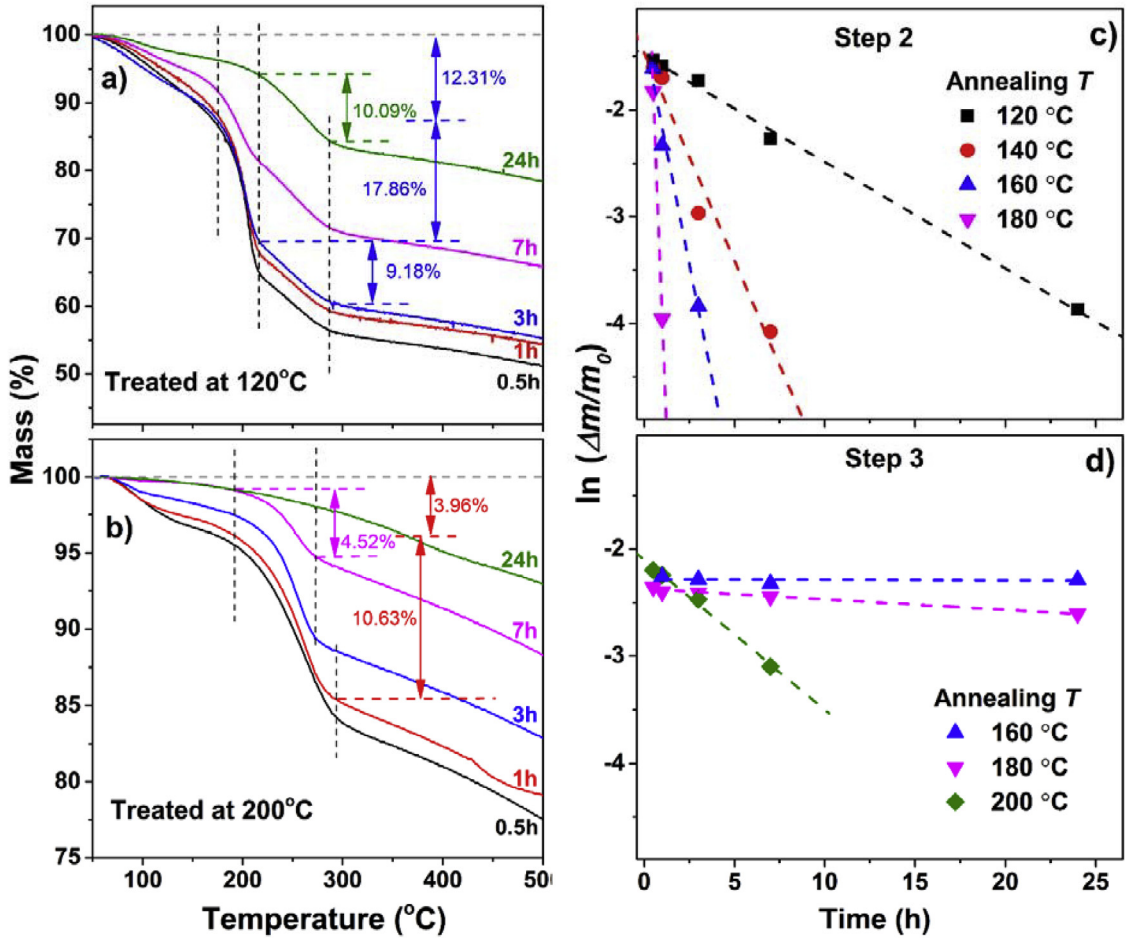

Fig. 3. TG data of annealed GO samples. (a) 120 °C; (b) 200 °C. The vertical dashed lines indicate the three steps of the GO reduction. The horizontal grey dashed lines (axis Y = 100) are the baseline for mass loss calculation. (c) Mass loss for Step 2. The dashed lines are linear fits. The 120 °C-0.5 h sample undergoes almost the same large mass loss as original GO's. (d) Mass loss for Step 3. The dashed lines are linear fits. The data of 120 and 140 °C annealed samples are not shown as they are similar to those of 160 °C annealed samples. (A colour version of this figure can be viewed online.)

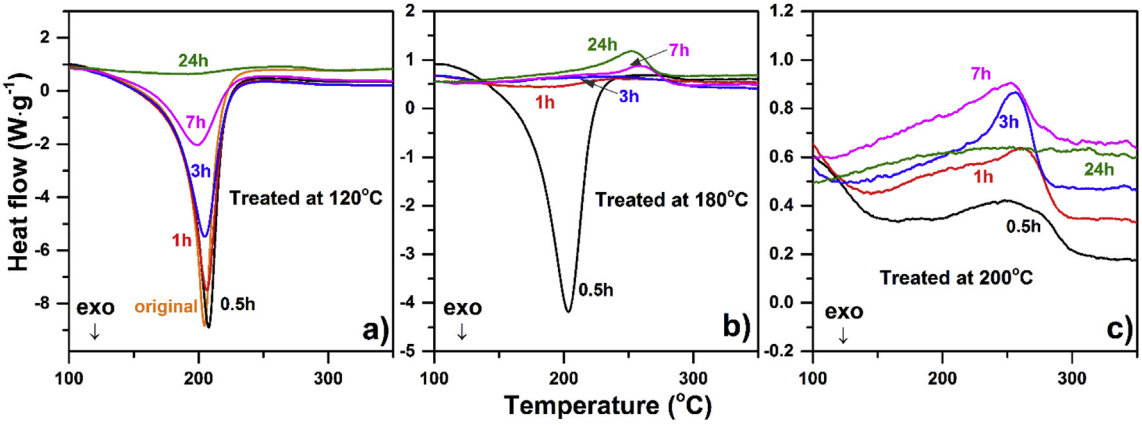

Fig. 4. DSC data of graphene oxide samples at 3 kinds of annealing temperature: (a) original and 120 °C; (b) 180 °C; (c) 200 °C. Fig. 4 shows that the peak area (i.e., enthalpy of decomposition) decreases with increasing the annealing time at three different temperatures. Under 120 °C-0.5 h condition, the exothermic peak area is almost as large as that of the original GO's. When GO is annealed at 200 °C, even for 0.5 h, the exothermic peaks has already disappeared (shown in Fig. 4c). As shown in Fig. SI5, an increase of annealing temperature could facilitate the decomposition in a limited time. Longer time or higher temperature are the key factors for enhancing the decomposition. (A colour version of this figure can be viewed online.)

at lower temperature. This is why previous studies often ignored the endothermic process. Annealing at 160 °C causes a reduction of mass loss of Step 1 and Step 2 and decrement of the area of the corresponding DSC peaks. On the contrary, the mass loss of Step 3 does not obviously show changes after annealing. This is a strong indication that the Step 3 is decoupled from Step 2.

To examine the effect of the heating rate on the characteristic temperatures of chemical reactions, we preformed additional DSC-TGA experiments on both original GO and 160 °C-24 h samples by using the heating rates of 5 and 15 °C/min (see Fig. SI1 in supporting information). The results show that the heating rate does not influence the occurrence of the 4 distinct reduction steps. An increase of the heating rates from 5 to 15 °C/min causes a slight shift of the reaction temperatures to a higher value, but do not alter the range of the main reaction temperatures.

3.2. GO reduction kinetics

Following these observations, different degradation mechanisms are investigated by Isothermal Gravimetric Analysis. The degree of degradation here is defined as the fractional mass loss (ρ) of the sample in respect to the original GO. Fig. 2a shows the time, t, spent to reach a certain degree of degradation as a function of ρ at five different temperatures. As expected, the isotherms in Fig. 2a have different slops, since the higher temperature treatment results in faster degradation of GO. Nevertheless, all the curves present slope changes at two characteristic ρ values: namely $\rho = 0.16$ and $\rho = 0.36$, thus confirming the presence of different degradation steps, which have been discussed in Fig. 1. A good agreement can be found between these ρ values and the dynamic thermogravimetric measurement of the original GO sample in Fig. 1b, for which similar relative mass loss values can be observed at the transition from Step 1 to Step 2, and from Step 2 to Step 3. Hence, we can infer that the mass loss at $\rho \leq 0.16$ corresponds to the vaporization of water, and that higher ρ correspond to the two distinct degradation processes we observed.

The apparent activation energy, E_a, for such degradation processes is calculated from the isotherms in Fig. 2a, by the MacCallum method [36,37], according to which the degradation time (t) can be expressed as follow:

$$t = f(\rho) \cdot A \cdot \exp\left(E_{a/RT}\right) \quad (1)$$

Where $f(\rho)$ is an undefined function of the GO degradation, A is the pre-exponential factor, and R is the universal gas constant.

The resulting E_a vs ρ curve is shown in Fig. 2b. E_a appears to increase with the degradation process. This can be explained by the fact that the most liable groups are the first to be degraded during the thermal treatment. However, the apparent activation energy is nearly constant ($E_a = 112 \pm 6$ kJ·mol^{-1}) during the $0.16 < \rho \leq 0.36$ degradation step. On the contrary, E_a abruptly increases for ρ between 0.36 and 0.41, and reach a stable value of 248 ± 9 kJ·mol^{-1} for $\rho > 0.41$.

In order to understand the nature of the groups that are degraded during the heat treatment, the atomic composition of samples at different ρ is reported in Fig. 2c. These values are obtained by the Elemental Analysis of GO samples treated at 200 °C for different duration times (shown in Table SI2 in support information). It is clear that for a degradation degree below 0.36 the concentration of oxygen atoms (O) decreases, while the concentration of carbon atoms (C) increases, as the most liable oxygen

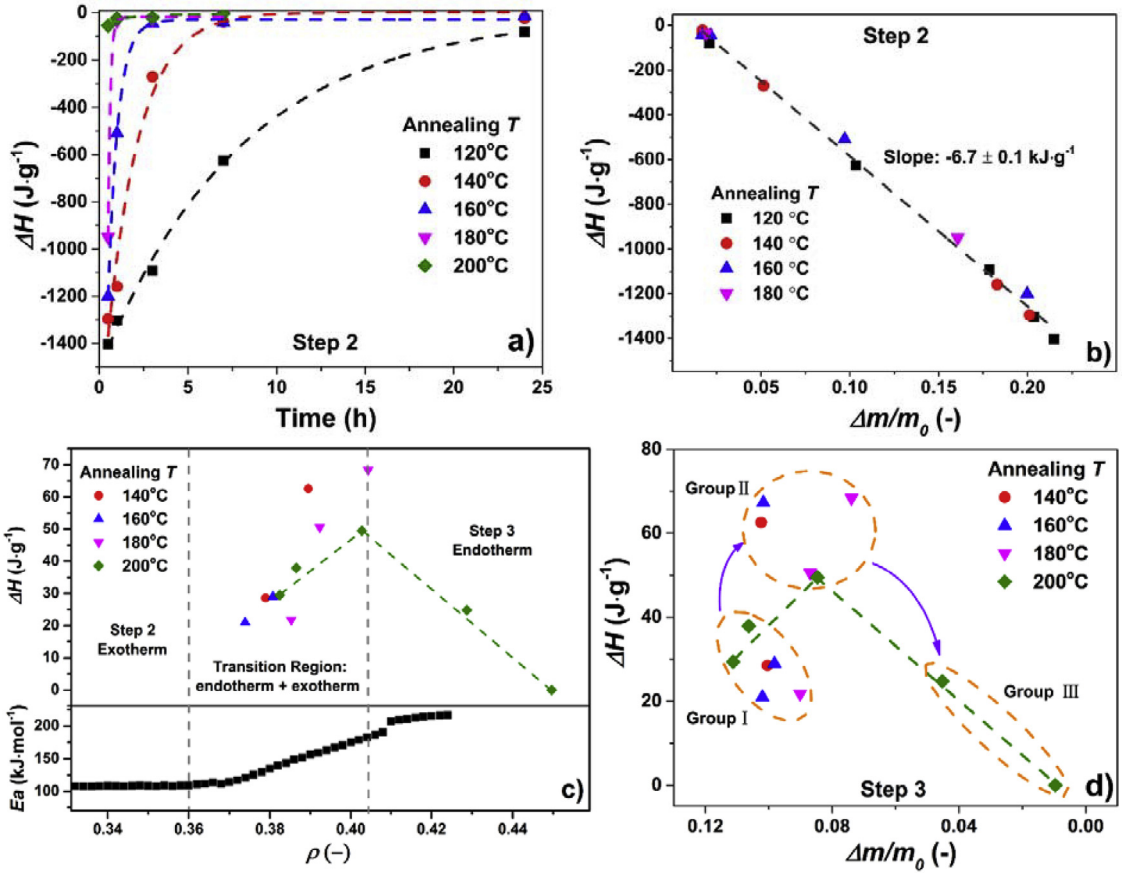

Fig. 5. The calculated enthalpy (ΔH) of each GO sample. (a) ΔH for Step 2, the exothermic peak. The dashed lines are exponential fits. (b) Relationship between ΔH and mass loss for Step 2. The dashed line is the linear fit. (c) ΔH for Step 3, the endothermic peak, combined with activation energy plot. The dashed linear line are the guide for eyes. (d) Relationship between ΔH and mass loss for Step 3. The dashed circles and the dashed linear line are the guide for eyes. The arrows indicate the trends. (A colour version of this figure can be viewed online.)

functional groups are degraded (GO thermal reduction). The elemental analysis shows that, as expected, the original GO, which is synthetized by a modified Hummers' method, contains a large quantity of sulfur (S), which might exist in the form of sulfates. At the beginning of the heat treatment, the concentration of S atoms slightly increases, because of the degradation of other more liable functional groups. However, the atomic concentration of S decreases for $\rho > 0.36$ until no sulfur is detected at $\rho = 0.457$ (sample annealed at 200 °C for 24 h). Therefore, the mass loss in the interval $0.36 < \rho < 0.457$ (Step 3 in Fig. 1) must be related to degradation of S-containing moieties. However, as shown in the elemental analysis data, the atomic content of S is less than 3.2 atom% in original GO sample (similar with the former research's results ref.43). Even if all S are released in the form of SO_2, the mass loss of Step 3 ($0.36 < \rho < 0.457$) still could not reach around 10% (as calculated from Fig. 2c). Therefore, we infer that other moieties could be degraded during this step. Thus, the large variation of E_a values observed during this degradation step can be ascribed to the complexity of the functional groups that are degraded.

The above-mentioned observations are further confirmed by Dynamic Thermogravimetric Analysis (at heating rate of 10 °C/min) of GO samples annealed at 120, 140, 160, 180 and 200 °C for a duration between 0.5 and 24 h. For simplicity, only the TG curves of the samples annealed at 120 and 200 °C are depicted in Fig. 3a–b, while the other data are reported in Fig. SI3 in supporting information. As we discussed above, the decomposition mechanism of Step 2 and Step 3 are not the same, which might be related to different degradation processes or to the degradation of different kinds of functional groups. In Fig. 3a, at 120 °C, the relative mass loss of Step 1 and Step 2 ($\Delta m/m_0$, Δm is the mass loss, m_0 is the starting mass in respect to the annealed sample) decreases from about 30% to nearly 0%, with the annealing time increasing from 0.5 to 24 h. On the contrary, the mass loss observed for the Step 3 keeps around 10% for all the samples annealed at 120 °C (the approximate value as in the Isothermal Gravimetric Analysis). At the relatively high annealing temperature, e.g., 200 °C (Fig. 3b), the irreversible desorption and decomposition phenomena in Step 1 and Step 2 occur quickly (Δm is less than 5% even in the sample 200 °C-0.5 h). The mass loss during Step 3 instead starts to decrease from 11% to nearly 0% with annealing time from 0.5 to 24 h. TG data are used to determine the apparent rate constant of the decomposition processes in Step 2 and Step 3, as shown by the dashed linear lines in Fig. 3c–d. The decomposition of functional groups in Step 2 takes 24 h at 120 °C, while it takes about 1 h at 180 °C (Fig. 3c). For Step 3 (Fig. 3d), there is no significant change of mass loss (remains around 10%) when annealing temperature is below 180 °C. However, at 200 °C, $\Delta m/m_0$ of Step 3 shows big decrement, and it becomes close to 0% after 24 h annealing. This is in agreement with the calculated E_a values in Isothermal Gravimetric Analysis (Fig. 2b). Step 3 has a much higher activation energy than Step 2.

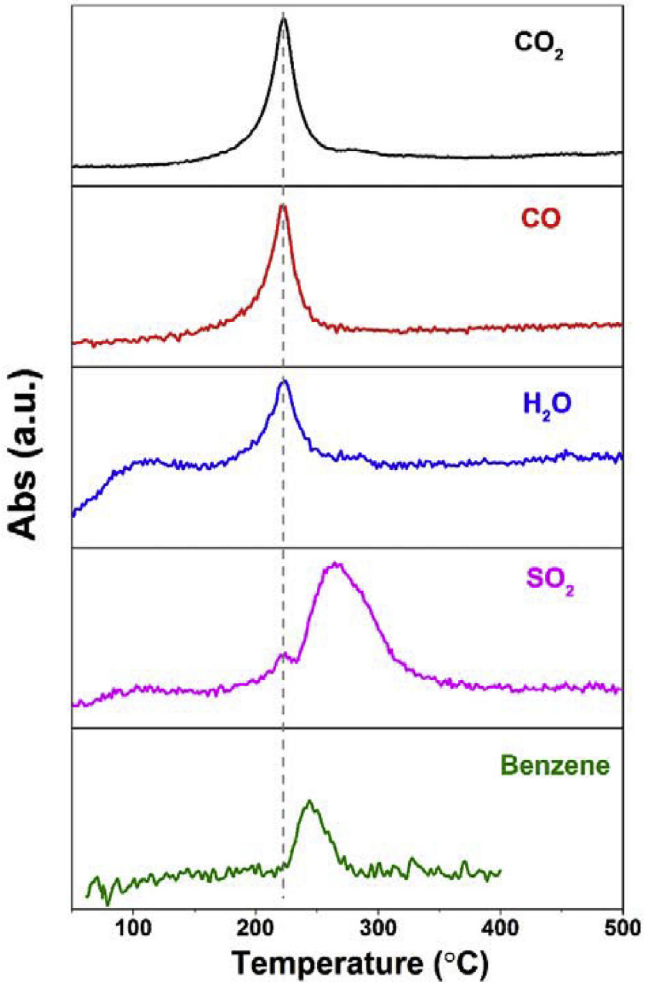

Fig. 6. FTIR-TG-MS data of the original GO. The grey dashed line is for visual. (A colour version of this figure can be viewed online.)

3.3. GO reduction thermodynamics

Fig. 4 (and Figs. SI4 and Fig. SI5 in the supporting information)

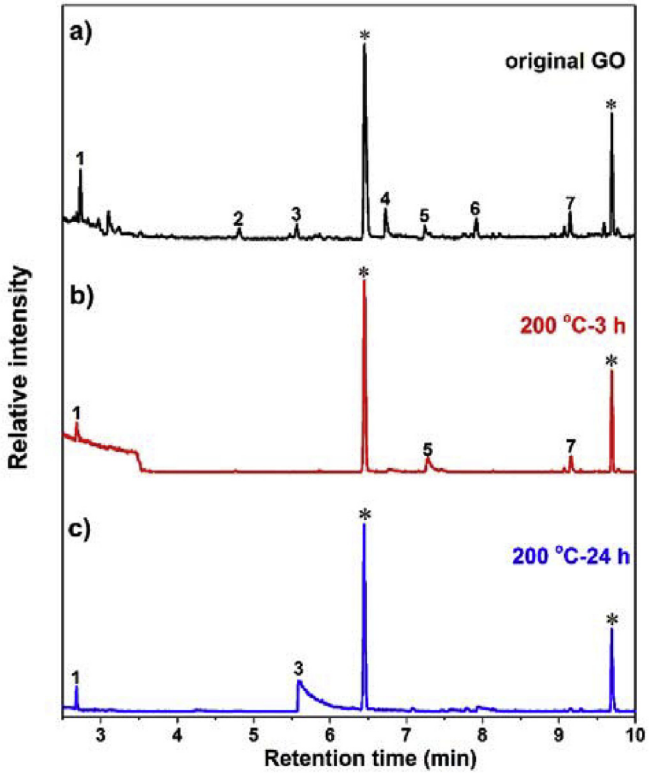

Fig. 7. Pyr-GC-MS data of 3 GO samples: (a) the original GO sample; (b) GO sample annealed at 200 °C for 3 h; (c) GO sample annealed at 200 °C for 24 h. Peaks marked with * are due to the instrument column. The remaining marked peaks: 1: Benzene, 2: Toluene, 3: *N,N*-dimethyl-formamide, 4: 2-Furancarboxyaldehyde, 5: 2,5-Furandione, 6: Styrene, 7: Benzaldehyde. (A colour version of this figure can be viewed online.)

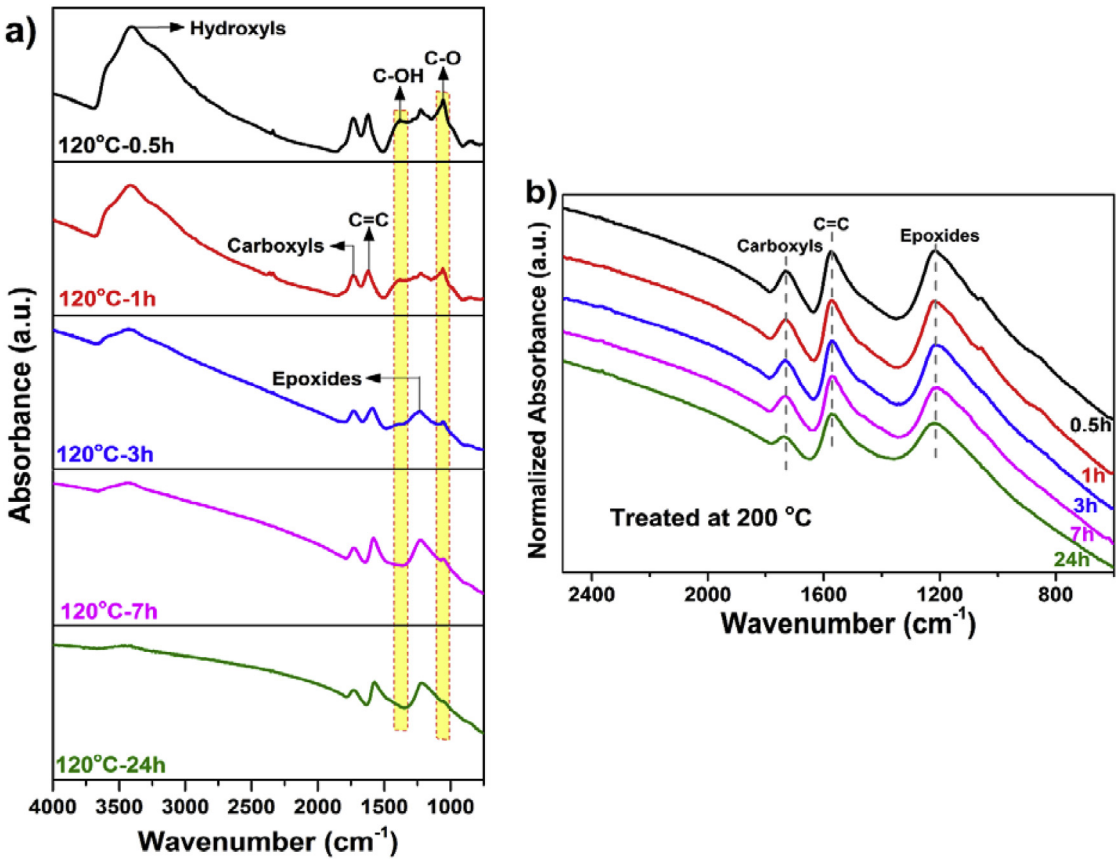

Fig. 8. FTIR spectra of annealed GO: (a) Absorbance spectra of the 120 °C annealed GO samples: hydroxyl and intercalated water (around 3400 cm^{-1}), carboxyl (1730 cm^{-1}), C=C (1620 cm^{-1}), C-OH (1380 cm^{-1}), epoxide (1225 cm^{-1}) and C-O (1050 cm^{-1}) [32,49,50]. The yellow stripes highlight the change of the peak intensity. (b) Normalized absorbance spectra of the 200 °C annealed GO samples. The grey dashed lines mark peak positions. (A colour version of this figure can be viewed online.)

shows the DSC data (at heating rate of 10 °C/min) of annealed GO samples at different temperatures and durations. In Fig. 4a, the curve of the original GO sample shows an exothermic peak centered at 210 °C, with onset from 100 °C and end at 250 °C, which is associated with the decomposition of the oxygen functional groups, as discussed above. Fig. 4b shows that the peak area decreases with the annealing time at 180 °C, and after 24 h annealing, only a small endothermic peak could be observed. The presence of this endothermic peak is even more evident for the sample annealed at 200 °C. Meanwhile, in this case, the GO sample annealed for 0.5 h shows no exothermic processes. After 24 h annealing at 200 °C, the endothermic peak totally disappears. This observation is consistent with the TG curve in Fig. 3b. The comparison of the TG and DSC curves shows that both Step 2 and Step 3 are associated with the mass loss, i.e. with the changing of GO sample composition. However, Step 2 is strongly exothermic while Step 3 is overall weakly endothermic. This finding corrects the traditional point of view that the low temperature reduction of GO involves only a single exothermic step.

By using a sapphire reference in the DSC measurements, the enthalpy (ΔH) of each GO sample for different steps is calculated (Fig. 5). The exponential fitting curves (based on the equation: $y = a*(1 - e^{-bx})^c$) for the enthalpy change in Fig. 5a exhibit trends similar to those for the mass loss. This indicates that the more functional groups decompose from GO samples, the more energy is released. The enthalpy of 6.7 ± 1 kJ per gram of GO released during Step 2 is calculated by fitting the data in Fig. 5b. Compared with Step 2, the absolute values of ΔH of the endothermic peaks (Step 3) are much smaller, as shown in Fig. 5c. Taking the mass loss into consideration, for example, in the 160 °C-24 h GO sample, around 10% mass loss of Step 3 corresponds to $\Delta H \approx 67$ J/g, while in the 160 °C-1 h GO sample, about 10% mass loss of Step 2 corresponds to $\Delta H \approx -508.8$ J/g. Moreover, for the samples treated below 180 °C, the gained enthalpy during Step 3 increases with the annealing time. The ΔH of annealed GO at 200 °C shows the same trend in the first half (from Group I to Group II), later the ΔH would decreases with the annealing time (from Group II to Group III). Here we combine with the E_a and argue that (Fig. 5c): At first, there is a transition region, which consist of both exothermic and endothermic processes. The extent of exotherm decrease, while the relative extent of endotherm increase, resulting in the increment of the ΔH (from Group Ito Group II). Later, the extent of endotherm continues to decrease with annealing time, leading to the decrement of the ΔH (from Group IIto Group III). Step 3 is the sum of different processes and the consequence is the appearance of a small endothermic peak.

To find out what happened in the observed steps of mass loss, we take some previous studies into consideration, where the 3 steps of decomposition are also observed [33,38–46], and find out that Step 3 occurs only in GO synthesized by Hummers' method. However, most of those studies ignore the distinction of these reaction steps, generalize Steps 2 and 3 as one-step, and attribute it to the removal of labile oxygen groups. Some researchers [33,39] ascribed Step 3 to the decomposition of some more stable oxygen functional groups. Others [41,44] infer that Step 3 is related to the release of sulfur species. However, at our best knowledge no one has reported that Step 3 involves an endothermic response.

3.4. GO reduction by-products

A combined FTIR-TG-MS analysis is conducted to gain more information about the GO thermal reduction process at low temperature. The results are shown in Fig. 6. The released gases during GO reduction indicate that Step 1 (below 160 °C) involves mainly the desorption of the nano-confined water between GO sheets. The mass loss of Step 2 (160–210 °C) is mainly caused by the release of CO, CO_2 and H_2O, whereas Step 3 (210–300 °C) is related to the SO_2. To further confirm the correlation of Step 3 with the sulfate content, a GO sample with a sulfur content below 0.2 atom% (obtained by washing the raw GO powder for additional 15 times) was analyzed by using DSC and TGA, before and after annealing at 160 °C for 24 h (see Fig. SI6). The results clearly show that neither Step 3 transition, nor the corresponding endothermic peak occur in the TG and DSC curves, respectively. These results agree with literature data [41,44,47]. The benzene peak, centered at 250 °C, is also detected, which has not been reported to the best of our knowledge. The occurrence of this peak indicates that the basal carbon plane could decompose at relatively low temperature (between 210 and 300 °C), and this is in contrast to the view that the carbon plane would only degrade at relatively high temperature [35,48], e.g., above 350 °C. As we discussed above in the Elemental Analysis (Table SI2), the content of element S (less than 3.2 atom%) could not account for 10% mass loss (Fig. 2), and some aromatic by-products could be present in the samples.

To confirm that the 4–5% mass loss deficit (compared with the sulfur content) during Step 3 might come from the release of aromatic by-products, the original GO sample and two annealed GO samples (200 °C-3h and 200 °C-24 h) are measured at 300 °C for 20 s using Pyr-GC-MS (Fig. 7a–c). Besides the CO_2 and SO_2 products, a small amount of organic products are also detected: Benzene, Toluene, 2-Furancarboxyaldehyde, *N*,*N*-dimethyl-formamide, 2,5-Furandione, Styrene and Benzaldehyde. Most of the species of organic by-products are released from the original GO sample (Fig. 7a), involving Steps 1–3; whereas only benzene, 2,5-

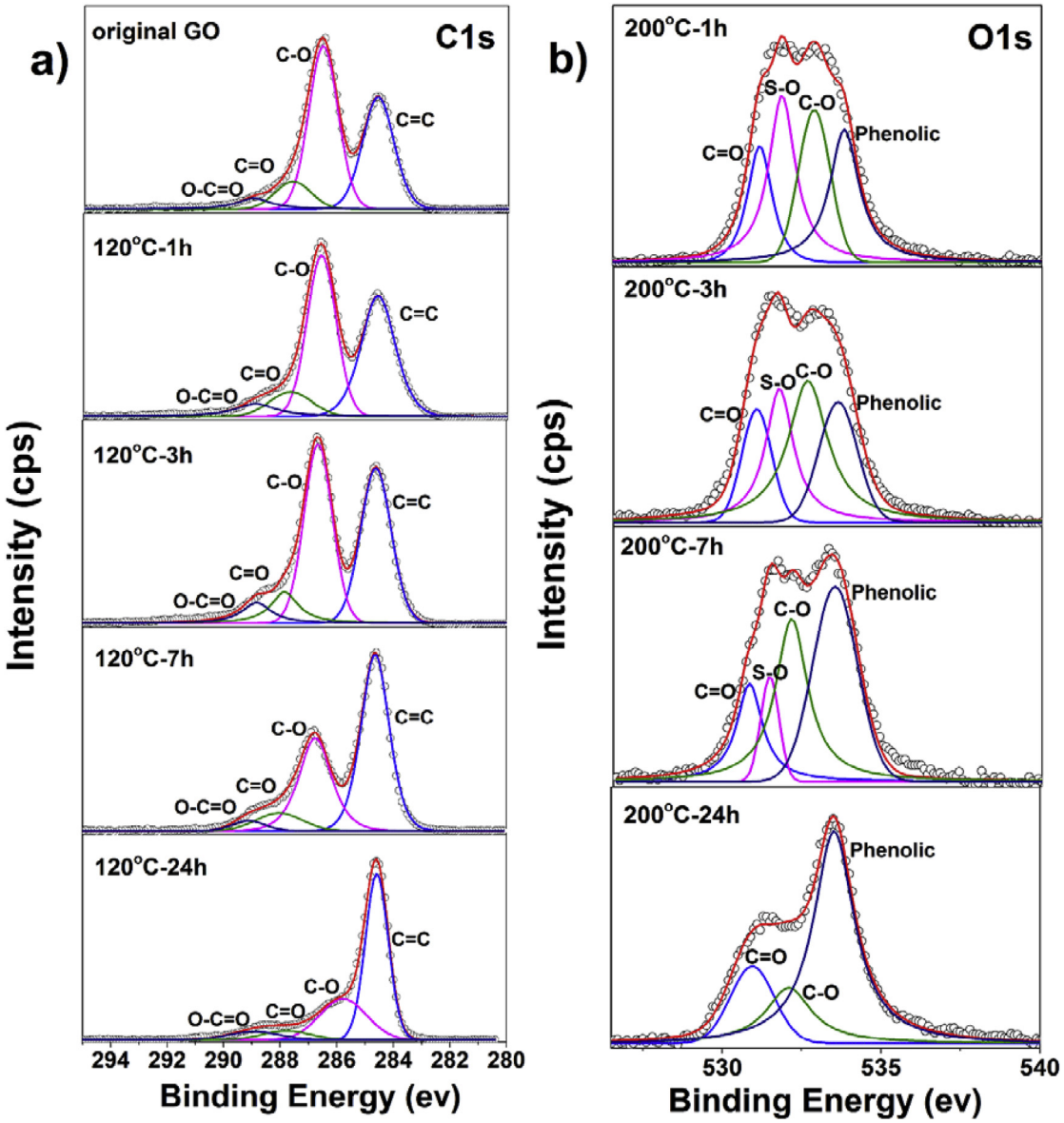

Fig. 9. High resolution XPS spectra of annealed GO samples: (a) C1s spectra of original GO and annealed GO at 120 °C. C=C (284.6 ev), C-O (286 ev), C=O (287.8ev), O-C=O (288.8 ev) [51,52]. (b) O1s spectra of annealed GO at 200 °C. C=O (531 ev), S-O (531.6 ev), C-O (532 ev), Phenolic (533.4 ev) [52,53]. Red solid curves: Sum of the convoluted Gaussian-Lorentzian bands (representing different bonds). (A colour version of this figure can be viewed online.)

furandione and benzaldehyde are observed in the 200 °C-3 h GO sample, involving only Step 3 (Fig. 7b). The absence of toluene, 2-furancarboxyaldehyde and styrene in 200 °C-3 h GO sample implies that the degradation of functional groups accompanies the decomposition of carbon network during heating in Pyr-GC-MS over time, leading to structural defects formation. In contrast, except benzene, most of organic products could not be detected in 200 °C-24 h GO sample (Fig. 7c), and this sample does not exhibit the mass loss of Steps 2 and 3. The generation of benzene in GO mainly depends on the temperature, and it is not strongly affected by the amount and species of functional groups. Our detection of organic products is consistent with some previous studies [43,48]. However, those studies are based on high temperature treatment (more than 400 °C). Our Pyr-GC-MS results confirm that some organic by-products can be released at much lower temperature, meaning that the carbon sheets could start to decompose below 300 °C.

3.5. Chemical evolution of GO reduction

After identifying the types of gases released from the 3 distinct steps, we reveal the reduction mechanisms of GO by tracing the evolution of functional groups using FTIR (Fig. 8). Fig. 8a exhibits the absorbance spectrum of GO annealed at 120 °C for various durations. At this temperature, the decomposition corresponds to Steps 1 and 2. The drastic decrease of the absorption at around 3400 cm^{-1} arises from the loss of hydroxyls (-OH) and intercalated water. It is also seen that the peaks at 1380 cm^{-1} and 1050 cm^{-1}, which correspond to the C-OH and C-O, respectively, become less pronounced with annealing time and finally disappear. The peak at 1730 cm^{-1} (carboxyl) also decreases with annealing time. The other two peaks (epoxide and C=C) vary only slightly. Fig. 8a shows that during Steps 1 and 2, dominant mass loss mostly result from the release of water and decomposition of C-OH and C-O. Fig. 8b shows the normalized spectra of the 200 °C annealed GO samples, which only relates to reaction Step 3. Similar to the 120 °C-24 h curve, three species of functional groups remain: C=C, epoxides and carboxyls. Even after 24 h annealing, the infrared absorbance are still detectable. These functional groups strongly bond to the basal graphene plane and are difficult to be removed at low temperatures. In Fig. 8a–b, the peak assignment to the bonds of sulfates could not be verified, but the existence of sulfates in GO has been proved by EA and GC-MS.

In order to gain insight into functional groups' chemical bonding evolution, XPS measurements are carried out as shown in Fig. 9. The XPS spectra of the 120 °C annealed GO samples for various times are shown in Fig. 9a, which relate to Steps 1 and 2. The areas of the fitted curves' C=C, C-O, C=O and O-C=O are listed in Table SI7, respectively. We can see that, the functional groups of epoxide and C-OH have the largest quantities (around 50% in original GO). During the reduction process of Steps 1 and 2, the decomposition of epoxide and C-OH is the main reason for the release of H_2O, CO and CO_2 (combined with Fig. 6). The concentrations of carboxyl and carbonyl groups do not change considerably at 120 °C treatment. This observation agrees with the FTIR results (Fig. 8) revealing the occurrence of the carboxyl bond even in the 200 °C annealed GO samples. Since the C1s XPS spectra of the 200 °C annealed GO samples' are similar to that of the 120 °C-24 h sample, here we show the O1s XPS spectra of the 200 °C annealed GO samples in Fig. 9b. The areas of the fitting curves for C=O, S-O, C-O and Phenolic are listed in Table SI8. It is clearly in Fig. 9b that the left-side peak fades with increasing the annealing time, possibly due to the reaction Step 3. The content of C=O (around 16%) varies only slightly, and it is quite stable at 200 °C. The S-O content decreases sharply from 31.91% to 0.00%. Furthermore, the C-O content first

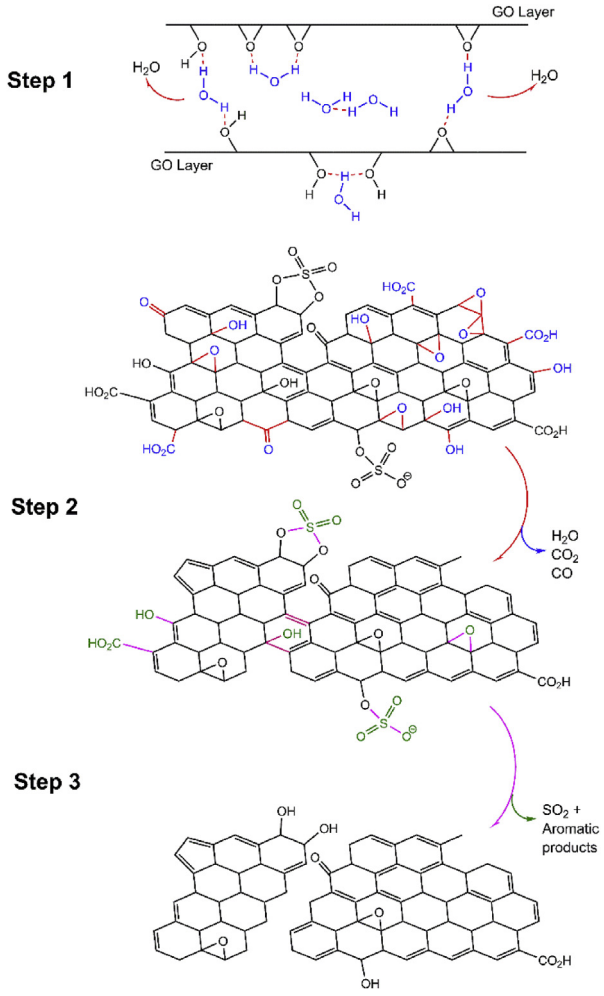

Fig. 10. Possible thermal reduction process of three distinct steps of Hummers' method GO. (A colour version of this figure can be viewed online.)

increases from 24.42% to 37.18% and then decreases to 19.00%, while the Phenols content decreases from 27.50% to 21.79% and then increases to 62.91%. This is due to the decomposition of sulfates [38,41]. The release of sulfates results in an increase of the fraction of C-O at first. However, the high temperature (200 °C) facilitates the reduction of C-O and thereby the C-O fraction decreases later. Besides, the decomposition of sulfates causes the formation of the vicinal diols (Fig. 10), which increases the Phenolic content fraction further.

Based on some previously proposed models of GO [27,34,38,49,54], the possible reduction mechanisms of the 3 distinct steps of modified Hummers' method GO are described in Fig. 10.

4. Conclusion

We have provided insight into the chemical evolution of Hummers' GO during the low temperature thermal reduction. Our results have demonstrated that the reduction processes of Hummers' GO consists of the following four steps. Step 1 (below 160 °C) leads to the release of the physisorbed water. Step 2 (between 160 and 210 °C) results in the reduction of functional groups. Step 3 (between 210 and 300 °C) causes the production sulfates, stable oxygens and aromatic by-products; Step 4 (above 300 °C), induced the degradation of the carbon network and the most stable oxygen

functionalities. Different from the conclusion in literature, in which the reduction process of Hummers' GO is regarded as a single exothermic process, we identify Step 3 to be an endothermic transition, which is decoupled from Step 2. In addition, we have found that the main decomposition steps (Steps 2 and 3) generate different kinds of products. During Step 2, CO, CO_2 and H_2O are produced, while during Step 3, SO_2 and some aromatic gases are obtained. The analysis of these products indicates that the GO carbon plane could decompose even at low temperature (below 300 °C). The kinetic results derived from FTIR and XPS measurements have been used to explore the evolution of functional groups during heat-treatment and its relationship to the released products. The epoxy and carboxyl groups are much more stable than the C-OH and C-O groups. S-O bond cannot be broken below 200 °C. Hence, this work indicates that the composition of the starting GO should be taken into account in the design and the large-scale fabrication of reduced-GO (rGO) products, as we observed that the sulfur content has an influence on the energy consumption and by-product formation of the thermal reduction process.

Acknowledgments

The authors wish to thank Francesco Turci (Universitá di Torino) for the FTIR-GC-MS measurements. Y. Shen appreciate the support of China Scholarship Council (NO. 201507565004). V. Boffa acknowledge the Danish Council for Independent Research for the financial support (project DFF–6111–00151).

Appendix A. Supplementary data

TG and DSC curves of annealed GO samples. EA profiles, XPS fitted data.

Supplementary data related to this article can be found at https://doi.org/10.1016/j.carbon.2018.05.018.

References

[1] A.K. Geim, K.S. Novoselov, The rise of graphene, Nat. Mater. 6 (2007) 183–191, https://doi.org/10.1038/nmat1849.
[2] J.S. Bunch, S.S. Verbridge, J.S. Alden, A.M. van der Zande, J.M. Parpia, H.G. Craighead, P.L. McEuen, Impermeable atomic membranes from graphene sheets, Nano Lett. 8 (2008) 2458–2462, https://doi.org/10.1021/nl801457b.
[3] B.G. Eda, M. Chhowalla, Chemically derived graphene oxide: towards large-area thin-film electronics and optoelectronics, Adv. Mater. 22 (2010) 2392–2415, https://doi.org/10.1002/adma.200903689.
[4] C. Lee, X. Wei, J.W. Kysar, J. Hone, Measurement of the elastic properties and intrinsic strength of monolayer graphene, Science 321 (2008) 385–388, https://doi.org/10.1126/science.1157996.
[5] J.E. Kim, T.H. Han, S.H. Lee, J.Y. Kim, C.W. Ahn, J.M. Yun, S.O. Kim, Graphene oxide liquid crystals, Angew. Chemie - Int. Ed. 50 (2011) 3043–3047, https://doi.org/10.1002/anie.201004692.
[6] F. Perreault, A.F. De Faria, M. Elimelech, Environmental applications of graphene-based nanomaterials, Chem. Soc. Rev. 44 (2015) 5861–5896, https://doi.org/10.1039/C5CS00021A.
[7] R. Sitko, E. Turek, B. Zawisza, E. Malicka, E. Talik, J. Heimann, A. Gagor, B. Feist, R. Wrzalik, Adsorption of divalent metal ions from aqueous solutions using graphene oxide, Dalt. Trans. 42 (2013) 5682–5689, https://doi.org/10.1039/c3dt33097d.
[8] G. Zhao, J. Li, X. Ren, C. Chen, X. Wang, Few-layered graphene oxide nanosheets as superior sorbents for heavy metal ion pollution management, Environ. Sci. Technol. 45 (2011) 10454–10462.
[9] Q. Xiang, J. Yu, M. Jaroniec, Graphene-based semiconductor photocatalysts, Chem. Soc. Rev. 41 (2012) 782–796, https://doi.org/10.1039/C1CS15172J.
[10] X. An, J.C. Yu, Graphene-based photocatalytic composites, RSC Adv. 1 (2011) 1426–1434, https://doi.org/10.1039/c1ra00382h.
[11] R.K. Joshi, P. Carbone, Feng Chao Wang, V.G. Kravets, Ying Su, I. V Grigorieva, H.A. Wu, A.K. Geim, R.R. Nair, Precise and ultrafast molecular sieving through graphene oxide membranes, Science 343 (2014) 752–754, https://doi.org/10.1126/science.1245711.
[12] J. Abraham, K.S. Vasu, C.D. Williams, K. Gopinadhan, Y. Su, C.T. Cherian, J. Dix, E. Prestat, S.J. Haigh, I.V. Grigorieva, P. Carbone, A.K. Geim, R.R. Nair, Tunable sieving of ions using graphene oxide membranes, Nat. Nanotechnol. 12 (2017) 546–550, https://doi.org/10.1038/nnano.2017.21.
[13] F. Schedin, A.K. Geim, S.V. Morozov, E.W. Hill, P. Blake, M.I. Katsnelson, K.S. Novoselov, Detection of individual gas molecules adsorbed on graphene, Nat. Mater. 6 (2007) 652–655, https://doi.org/10.1038/nmat1967.
[14] P. Chen, Y.X. Liu, X.C. Dong, Biological and chemical sensors based on graphene materials, Chem. Soc. Rev. 41 (2012) 2283–2307, https://doi.org/10.1039/c1cs15270j.
[15] M.D. Stoller, S. Park, Y. Zhu, J. An, R.S. Ruoff, Graphene-based ultracapacitors, Nano Lett. 8 (2008) 3498–3502.
[16] V. Boffa, H. Etmimi, P.E. Mallon, H.Z. Tao, G. Magnacca, Y.Z. Yue, Carbon-based building blocks for alcohol dehydration membranes with disorder-enhanced water permeability, Carbon 118 (2017) 458–466, https://doi.org/10.1016/j.carbon.2017.03.077.
[17] D.R. Dreyer, S. Park, C.W. Bielawski, R.S. Ruoff, The chemistry of graphene oxide, Chem. Soc. Rev. 39 (2010) 228–240, https://doi.org/10.1039/B917103G.
[18] S. Pei, H.M. Cheng, The reduction of graphene oxide, Carbon 50 (2012) 3210–3228, https://doi.org/10.1016/j.carbon.2011.11.010.
[19] O.C. Compton, S.T. Nguyen, Graphene oxide, highly reduced graphene oxide, and graphene: versatile building blocks for carbon-based materials, Small 6 (2010) 711–723, https://doi.org/10.1002/smll.200901934.
[20] B.Y. Zhu, S. Murali, W. Cai, X. Li, J.W. Suk, J.R. Potts, R.S. Ruoff, Graphene and graphene oxide: synthesis, properties, and applications, Adv. Mater. 22 (2010) 3906–3924, https://doi.org/10.1002/adma.201001068.
[21] X. Huang, Z. Yin, S. Wu, X. Qi, Q. He, Q. Zhang, Graphene-based materials: synthesis, characterization, properties, and applications, Small 7 (2011) 1876–1902, https://doi.org/10.1002/smll.201002009.
[22] S. Guo, S. Dong, Graphene nanosheet: synthesis, molecular engineering, thin film, hybrids and energy and analytical applications, Chem. Soc. Rev. 40 (2011) 2644–2672, https://doi.org/10.1039/c0cs00079e.
[23] C. Zhang, W. Lv, Q. Yang, Towards low temperature thermal exfoliation of graphite oxide for graphene production, Carbon 62 (2013) 11–24, https://doi.org/10.1016/j.carbon.2013.05.033.
[24] W. Lv, D. Tang, Y. He, C. You, Z. Shi, X. Chen, Low-temperature exfoliated graphenes: vacuum-promoted exfoliation and electrochemical energy storage, ACS Nano 3 (2009) 3730–3736, https://doi.org/10.1021/nn900933u.
[25] A. Kaniyoor, T.T. Baby, S. Ramaprabhu, Graphene synthesis via hydrogen induced low temperature exfoliation of graphite oxide, J. Mater. Chem. 20 (2010) 8467, https://doi.org/10.1039/c0jm01876g.
[26] B. Shen, D. Lu, W. Zhai, W. Zheng, Synthesis of graphene by low-temperature exfoliation and reduction of graphite oxide under ambient atmosphere, J. Mater. Chem. C 1 (2013) 50–53, https://doi.org/10.1039/C2TC00044J.
[27] R.R. Nair, H.A. Wu, P.N. Jayaram, I.V. Grigorieva, A.K. Geim, Unimpeded permeation of water through helium-leak-tight graphene-based membranes, Science 335 (2012) 442–444, https://doi.org/10.1126/science.1211694.
[28] G. Eda, Y.Y. Lin, C. Mattevi, H. Yamaguchi, H.A. Chen, I.S. Chen, C.W. Chen, M. Chhowalla, Blue photoluminescence from chemically derived graphene oxide, Adv. Mater. 22 (2010) 505–509, https://doi.org/10.1002/adma.200901996.
[29] W.S. Hummers, R.E. Offeman, Preparation of graphitic oxide, J. Am. Chem. Soc. 80 (1958), https://doi.org/10.1021/ja01539a017, 1339–1339.
[30] W. Zhang, Y. Li, S. Peng, Facile synthesis of graphene sponge from graphene oxide for efficient dye-sensitized H_2 evolution, ACS Appl. Mater. Interfaces 8 (2016) 15187–15195, https://doi.org/10.1021/acsami.6b01805.
[31] M.J. McAllister, J.L. Li, D.H. Adamson, H.C. Schniepp, A.A. Abdala, J. Liu, M. Herrera-Alonso, D.L. Milius, R. Car, R.K. Prud'homme, I.A. Aksay, Single sheet functionalized graphene by oxidation and thermal expansion of graphite, Chem. Mater. 19 (2007) 4396–4404, https://doi.org/10.1021/cm0630800.
[32] Y. Qiu, F. Collin, R.H. Hurt, I. Külaots, Thermochemistry and kinetics of graphite oxide exothermic decomposition for safety in large-scale storage and processing, Carbon 96 (2016) 20–28, https://doi.org/10.1016/j.carbon.2015.09.040.
[33] X. Fan, W. Peng, Y. Li, X. Li, S. Wang, G. Zhang, F. Zhang, Deoxygenation of exfoliated graphite oxide under alkaline conditions: a green route to graphene preparation, Adv. Mater. 20 (2008) 4490–4493, https://doi.org/10.1002/adma.200801306.
[34] K. Hu, X. Xie, T. Szkopek, M. Cerruti, Understanding hydrothermally reduced graphene oxide hydrogels: from reaction products to hydrogel properties, Chem. Mater. 28 (2016) 1756–1768, https://doi.org/10.1021/acs.chemmater.5b04713.
[35] J.I. Parades, S. Villar-Rodil, A. Martínez-Alonso, J.M.D. Tascón, Graphene oxide dispersions in organic solvents, Langmuir 24 (2008) 10560–10564, https://doi.org/10.1021/la801744a.
[36] J.R. MacCallum, Thermogravimetric analysis of polymers for assessing thermal degradation, Thermochim. Acta 96 (1985) 275–281, https://doi.org/10.1016/0040-6031(85)80068-X.
[37] A. Babanalbandi, D.J.T. Hill, D.S. Hunter, L. Kettle, Thermal stability of poly(-lactic acid) before and after γ-radiolysis, Polym. Int. 48 (1999) 980–984, https://doi.org/10.1002/(SICI)1097-0126(199910)48:10<980::AID-PI257>3.0.CO;2-B.
[38] A. Dimiev, D.V. Kosynkin, L.B. Alemany, P. Chaguine, J.M. Tour, Pristine graphite oxide, J. Am. Chem. Soc. 134 (2012) 2815–2822.
[39] K. Haubner, J. Murawski, P. Olk, L.M. Eng, C. Ziegler, B. Adolphi, E. Jaehne, The route to functional graphene oxide, ChemPhysChem 11 (2010) 2131–2139, https://doi.org/10.1002/cphc.201000132.
[40] G. Wang, J. Yang, J. Park, X. Gou, B. Wang, H. Liu, J. Yao, Facile synthesis and

characterization of graphene nanosheets, J. Phys. Chem. C 112 (2008) 8192–8195, https://doi.org/10.1021/jp710931h.
[41] S. Eigler, C. Dotzer, F. Hof, W. Bauer, A. Hirsch, Sulfur species in graphene oxide, Chem. A Eur. J. 19 (2013) 9490–9496, https://doi.org/10.1002/chem.201300387.
[42] P.V. Kumar, N.M. Bardhan, S. Tongay, J. Wu, A.M. Belcher, J.C. Grossman, Scalable enhancement of graphene oxide properties by thermally driven phase transformation, Nat. Chem. 6 (2013) 151–158, https://doi.org/10.1038/nchem.1820.
[43] O. Jankovský, M. Lojka, M. Nováček, J. Luxa, D. Sedmidubský, M. Pumera, J. Kosina, Z. Sofer, Reducing emission of carcinogenic by-products in the production of thermally reduced graphene oxide, Green Chem. 18 (2016) 6618–6629, https://doi.org/10.1039/C6GC02491B.
[44] S. Eigler, C. Dotzer, A. Hirsch, Visualization of defect densities in reduced graphene oxide, Carbon 50 (2012) 3666–3673, https://doi.org/10.1016/j.carbon.2012.03.039.
[45] W. Chen, L. Yan, P.R. Bangal, Chemical reduction of graphene oxide to graphene by sulfur-containing compounds, J. Phys. Chem. C 114 (2010) 19885–19890, https://doi.org/10.1021/jp107131v.
[46] J.H. Kang, T. Kim, J. Choi, J. Park, Y.S. Kim, M.S. Chang, H. Jung, K.T. Park, S.J. Yang, C.R. Park, Hidden second oxidation step of Hummers method, Chem. Mater. 28 (2016) 756–764, https://doi.org/10.1021/acs.chemmater.5b03700.
[47] S. Eigler, C. Dotzer, A. Hirsch, M. Enzelberger, P. Müller, Formation and decomposition of CO_2 intercalated graphene oxide, Chem. Mater. 24 (2012) 1276–1282, https://doi.org/10.1021/cm203223z.
[48] Z. Sofer, O. Jankovský, P. Šimek, D. Sedmidubský, J. Šturala, J. Kosina, R. Mikšová, A. Macková, M. Mikulics, M. Pumera, Insight into the mechanism of the thermal reduction of graphite oxide: deuterium-labeled graphite oxide is the key, ACS Nano 9 (2015) 5478–5485, https://doi.org/10.1021/acsnano.5b01463.
[49] A. Bagri, C. Mattevi, M. Acik, Y.J. Chabal, M. Chhowalla, V.B. Shenoy, Structural evolution during the reduction of chemically derived graphene oxide, Nat. Chem. 2 (2010) 581–587, https://doi.org/10.1038/nchem.686.
[50] T. Szabó, O. Berkesi, P. Forgó, K. Josepovits, Y. Sanakis, E. Al, Evolution of surface functional groups in a series of progressively oxidized graphite oxides, Chem. Mater. 18 (2006) 2740–2749, https://doi.org/10.1021/cm060258+.
[51] A. Nikolakopoulou, D. Tasis, L. Sygellou, V. Dracopoulos, C. Galiotis, P. Lianos, Study of the thermal reduction of graphene oxide and of its application as electrocatalyst in quasi-solid state dye-sensitized solar cells in combination with PEDOT, Electrochim. Acta 111 (2013) 698–706, https://doi.org/10.1016/j.electacta.2013.08.064.
[52] A. Ganguly, S. Sharma, P. Papakonstantinou, J. Hamilton, Probing the thermal deoxygenation of graphene oxide using high-resolution in situ X-ray-based spectroscopies, J. Phys. Chem. C 115 (2011) 17009–17019, https://doi.org/10.1021/jp203741y.
[53] F. Wu, J. Li, Y. Tian, Y. Su, J. Wang, W. Yang, N. Li, S. Chen, L. Bao, 3D coral-like nitrogen-sulfur co-doped carbon-sulfur composite for high performance lithium-sulfur batteries, Sci. Rep. 5 (2015) 13340, https://doi.org/10.1038/srep13340.
[54] A. Lerf, H. He, M. Forster, J. Klinowski, Structure of graphite oxide revisited, J. Phys. Chem. B 102 (1998) 4477–4482, https://doi.org/10.1021/jp9731821.